PROGRESS IN COLOR, COLORANTS AND COATINGS

available online @ www.pccc.icrc.ac.ir

*Progress in Color Colorants Coating 19 (2026), 67-82*

Ministry of Science, Research and Technology
Institute for Color Science & Technology

# Natural Corrosion Inhibitor from Cistanche Tubulosa Extract for Carbon Steel in HCl: Gravimetric and Electrochemical Characterization

**A. Talfana[1], S. Kerouad*[1], I. Forsal[1], W. Kotmani[1], L. Kabiri[1], A. ElHarami[1], M. Ghazoui[2]**

[1.] Department of Process Engineering, Higher School of Technology, Sultan Moulay Slimane University, P.O. Box: 23000, Beni-Mellal, Morocco.

[2.] Department of Chemistry and Environment, Faculty of Science and Technology, Sultan Moulay Slimane University, P.O. Box: 23000, Beni-Mellal, Morocco.

ARTICLE INFO

Article history:
Received: 24 Apr 2025
Final Revised: 18 July 2025
Accepted: 21 July 2025
Available online: 07 Oct 2025

Keywords:
Corrosion inhibitor
Carbon steel
Electrochemical analyses
Cistanche tubulosa
Natural extract

## ABSTRACT

*The escalating environmental concerns associated with toxic inorganic inhibitors have spurred the exploration of green alternatives for Oxidation prevention in acid pickling processes. The corrosion behavior of Carbon steel (CS) in 1 M HCl solution was investigated via weight loss (WL), potentio-dynamic polarization (PDP), and electrochemical impedance spectroscopy (EIS) techniques. The influence of the eco-friendly corrosion inhibitor, cistanche tubulosa (CT), was evaluated. PDP measurements indicated that cistanche tubulosa exhibits mixed-type inhibitory properties, effectively reducing the corrosion rate of CS through adsorption onto its surface. This inhibitory effect resulted in an inhibition efficiency with a value higher than 92 % at 298 °K. The Langmuir isotherm model is the most acceptable one to describe the adsorption of extract on the surface of carbon steel. Scanning electron microscopy (SEM) was employed to characterize the morphology of the CS surface, confirming the layering of the barrier film on the CS surface and suggesting a chemisorption mechanism for cistanche tubulosa molecules. Additionally, Fourier-transform infrared spectroscopy (FTIR) analysis was performed to identify the functional groups responsible for the adsorption process. The temperature's influence on the anticorrosive efficiency was examined within the temperature interval of 298-328 °K. Results demonstrated an improvement in the ability to inhibit corrosion with an increase in inhibitor concentration and contact time, but this improvement decreased with increasing temperature. Prog. Color Colorants Coat. 19 (2026), 67-82© Institute for Color Science and Technology.*

## 1. Introduction

Mild steel, widely utilized across many industrial applications owing to its robustness and economic viability, exhibits high susceptibility to corrosion, particularly during cleaning processes and scale removal using mineral acids [1, 2]. This susceptibility leads to a reduction in the material's service life. Addressing this challenge underscores the need to develop innovative cleaning technologies that not only effectively preserve mild steel but also provide robust protection against corrosion, thereby ensuring its long-term durability and sustainability. Several strategies have been implemented to mitigate metal corrosion, primarily by minimizing the exposure of metal surfaces to corrosive environments. Among these approaches, plant extracts, when used as corrosion inhibitors, have become a focus of great

*Corresponding author: * sofia.kerouad@usms.ac.ma
**https://doi.org/10.30509/pccc.2025.167509.1383**

interest due to their effectiveness and environmental friendliness [3-5]. These plant extracts, referred to as green corrosion inhibitors, are highly regarded due to their natural and biodegradable qualities, offering a sustainable alternative to toxic inhibitors. Plant extracts establish a protective barrier over the metal surface. This barrier effectively obstructs corrosive agents from attacking and inducing damage [6].

The efficacy of these extracts as corrosion inhibitors is directly related to the complexity and variety of their constituent chemical species, which contain various active constituents that have an affinity for the metal surface, thereby enhancing protection. Among the diverse array of anti-corrosion agents, plant extracts have demonstrated superior inhibition performance at low concentrations [7]. This exceptional performance can be attributed to their ability to develop a robust and durable film covering the metal, as well as their environmentally friendly nature.

The phytochemicals produced by leaves through photosynthesis are essential in the creation of this protective barrier. These phytochemicals are characterized by polar functional groups, specifically amide, hydroxyl, ester, carboxylic acid, and amino groups, which facilitate their adsorption [8, 9]. However, a significant limitation of this class of inhibitors is the uncertainty regarding the specific constituent responsible for their inhibitory activity. Researchers have, across a multitude of studies, investigated the practical uses of natural extracts, originating from plants, weeds, shrubs, and herbs, as renewable inhibitors for the protection of CS and other metals [10]. Lavanya et al. reported 88.9 % inhibition efficiency using Pterocarpus marsupium extract [11]. Pahuja et al. achieved 97.5 % efficiency with Cuscuta reflexa [12]. Doumane et al. obtained 95.8 % efficiency using Citrullus colocynthis seed oil extract [13]. Berrissoul et al. recorded 90 % inhibition with *Artemisia Stems* extract [14]. Kotupalli et al. reached 90.98 % using Plumeria rubra extract [15]. Ezugha et al. confirmed the inhibitory effect of Solanum macrocarpon reached 91.4 % [16]. Ezzat et al. observed 90.5% inhibition with silver nanoparticles based on Anacardium occidentale leaf extract [17].

Cistanche tubulosa is a perennial, holoparasitic herb characterized by fleshy, yellowish to yellow-brown stems that often exhibit a purplish hue. Plants typically range in height from 15 to 40 cm. The stem is simple, erect, and varies from glabrous to sparsely puberulous, frequently broader at the base. It is densely covered with overlapping, triangular to lanceolate scale-like leaves, each measuring 1-4 cm in length. The inflorescence forms a dense and conspicuous cylindrical spike, measuring 10-20 cm in length. Flowers are tubular, ranging from bright yellow to pinkish-yellow or violet, and measure 3-4.5 cm in length. The calyx comprises five oblong-ovate lobes, 1-1.5 cm long. The corolla is funnel-shaped, extending 4-5 cm in length. Staminal filaments are accompanied by densely hairy anthers, which are woolly at the base and exhibit rounded to blunt apices. The fruit is an ovoid-oblong capsule, laterally compressed, 20-25 mm long, beaked at the tip, and contains numerous seeds. The seeds are dark-colored, pitted, and approximately 1 mm in length [18-20].

In this study, Cistanche tubulosa extract was prepared by ethanol maceration, followed by concentration through evaporation. The anticorrosive efficiency of this natural extract was evaluated for the protection of carbon steel in 1 M HCl solution using a combined approach, including gravimetric tests (weight loss), electrochemical analyses (potentio-dynamic polari-zation and electrochemical impedance spectroscopy), as well as surface characterizations by scanning electron microscopy (SEM) and Fourier-transform infrared spectroscopy (FTIR). The influence of various experimental parameters, including inhibitor concentration, temperature, and immersion time, was systematically investigated to gain a deeper understanding of the adsorption behavior and inhibition mechanism of the plant extract on the carbon steel surface.

## 2. Experimental

### 2.1. Inhibitor preparation

In March 2024, Cistanche tubulosa leaves were collected from the Azilal mountains in Morocco. After drying in the shade for 10 days, the leaves were ground into a fine powder. This powder was then subjected to maceration in ethanol for 24 hrs. The resultant solution was filtered to separate the extract from the plant residues. The resulting filtration was then concentrated by rotary evaporation to remove the ethanol, yielding a concentrated extract in the form of a black powder.

### 2.2. Samples and corrosion medium

In this work, a carbon steel (CS) sample with the following elemental composition (wt. %) was

investigated: C(0.19), Si(0.20), Mn(0.81), S(0.0027), Cr(0.12), P(0.001), Ni(0.11), Cu(0.18), Al(0.032), and Fe (balance). A 1 M HCl aggressive solution was obtained by diluting concentrated hydrochloric acid (37 %, Sigma-Aldrich). For electrochemical tests, 0.5 $cm^2$ CS samples were polished with #400 to #2000 SiC paper, rinsed, degreased, and air-dried. The 1 M HCl solution was then used with various concentrations of inhibitory substances for each test.

### 2.3. Weight loss method

The efficacy of a potential corrosion inhibitor was assessed using a weight loss method. CS specimens with a surface area of 12 $cm^2$ were immersed in 1 M HCl for a predetermined duration to assess the inhibitor's performance. Prior to immersion in 100 mL of 1M HCl solution, quantitatively varied concentrations, the specimens were carefully cleaned and weighed. After exposure, the specimens were meticulously cleaned (distilled water and acetone), then dried. The change in weight (Δm) of each specimen was calculated in milligrams to evaluate the inhibitor's effectiveness under aerated conditions. The rate of metal loss ($W_{corr}$) and inhibition efficiency ($E_w$ %) were obtained through the application of equations 1 and 2 [21, 22]:

$$W = \frac{\Delta m}{S.t} \quad (1)$$

$$E_W\% = \frac{W_{corr} - W_{corr(inh)}}{W_{corr}} \times 100 \quad (2)$$

In these equations, Δm (mg) denotes the change in specimen weight resulting from immersion, $W_{corr}$ and $W_{corr(inh)}$ represent the corrosion weight loss rates ($mg/cm^2.h$) of CS in the reference test solutions and the solutions modified by inhibitor, in that order, S signifies the surface area of the CS specimen ($cm^2$), and t indicates the duration of contact (h).

### 2.4. Instrumentation

This study employed a three-electrode cell with an OrigaMaster electrochemical workstation (OrigaStat 100 potentiostat, manufactured by OrigaLys Electro-chem SAS, France) to monitor CS corrosion using EIS and PDP. A platinum counter electrode (surface area 1 $cm^2$) and a $Hg/Hg_2Cl_2/KCl_{sat}$ (SCE) reference electrode were used. Preliminary to the measurements, the CS as working electrode was immersed with the SCE in the solution for 0.5 hours to establish an equilibrium OCP.

EIS data were acquired at frequencies ranging from 100 kHz to 10 mHz with a 10 mV peak-to-peak sinusoidal potential. Analysis of the resulting impedance diagrams provided insights into various processes related to the impedance of corrosion capabilities of the investigated inhibitors. The percentage of protection (%) was subsequently determined based on the obtained impedance data. PDP techniques were used to capture current-potential curves within a potential range of -750 to -100 mV at a scan rate of 0.5 mV/s. Each electrochemical parameter given is the average value obtained from three independent tests conducted under equivalent conditions.

Fourier Transform Infrared spectroscopy (Thermo Scientific Nicolet IS50 spectrophotometer, manufactured in the USA) was used to identify the chemical interactions between pure leaf extracts and the CS surface in inhibited acidic solutions. FTIR spectra were acquired over the spectral range of 600-4000 $cm^{-1}$ to identify characteristic vibrational bands associated with the interaction of inhibitor molecules with the CS surface. By analyzing the spectral data, insights into the type of chemical bonds formed at the interface between CE and CTE can be gained.

The surface morphology of the specimen was characterized using SEM analysis (Model JSM-IT10, manufactured by JEOL Ltd., Japan) both before and after exposure to an aggressive medium of 1 M HCl for 24 hours. The study evaluated the optimal concentration of the reducing agent (CT) at 2.5 g/L in comparison to the aggressive medium alone. This analysis yielded detailed morphological information from SEM imaging.

## 3. Results and Discussion

### 3.1. FTIR analysis

Figure 1 provides the FTIR data for Cistanche tubulosa leaf extract. The vibrational spectrum reveals an absorption band centered at 3279 $cm^{-1}$ (O-H and N-H) [23], and the bands at 2924 $cm^{-1}$ and 2853 $cm^{-1}$ were due to $CH_2$ symmetric and asymmetric stretching. [24, 25], 1736 $cm^{-1}$ (C=O), 1682 $cm^{-1}$ (C=O,), 1645 $cm^{-1}$ (C=C), 1596 $cm^{-1}$ (C=C and C=N), 1513 $cm^{-1}$ (C=C), 1416 $cm^{-1}$(C-O-H), 1369 $cm^{-1}$(C-H), 1262 $cm^{-1}$(C-O), 1027 $cm^{-1}$ (C-N and C-O) [26]. Additionally, the defining absorption features of C-H of the aromatic and aliphatic groups are identified as being below 1000 $cm^{-1}$ [27]. These findings demonstrate that CTE exhibits

multiple functional groups, including hydroxyl and carbonyl groups, carbon-carbon double bonds, carbon-nitrogen double bonds, carbon-nitrogen bonds, carboxylic groups, and aromatic rings, all of which are considered key adsorption sites in effective corrosion protectors [28, 29].

### 3.2. Gravimetry weight loss

Gravimetric tests were performed to evaluate the reduction in CR and the associated inhibition efficiency (IE%) of Cistanche tubulosa leaf extracts on CS after a 6hrs immersion in 1 M HCl solutions at 298 °K. Figure 2 and Table 1 illustrate the variation of corrosion kinetics with four extract concentrations compared to the reference solution throughout the assessment. In the absence of inhibitors, the unprotected carbon steel showed the highest weight loss of 48.24 mg, corresponding to a CR of 0.67 mg/(cm$^2$.h). The introduction of CT extracts led to noticeable improvements, even at the lowest concentration tested, indicating the development of protective surface layers that inhibit steel oxidation. Further increases in extract concentration progressively decreased the corrosion rate, attaining the highest observed IE % of 85 % at 2.5 g/L. This concentration marked the point beyond which no significant improvement occurred, reasonably ascribed to saturation of available adsorption sites [30].

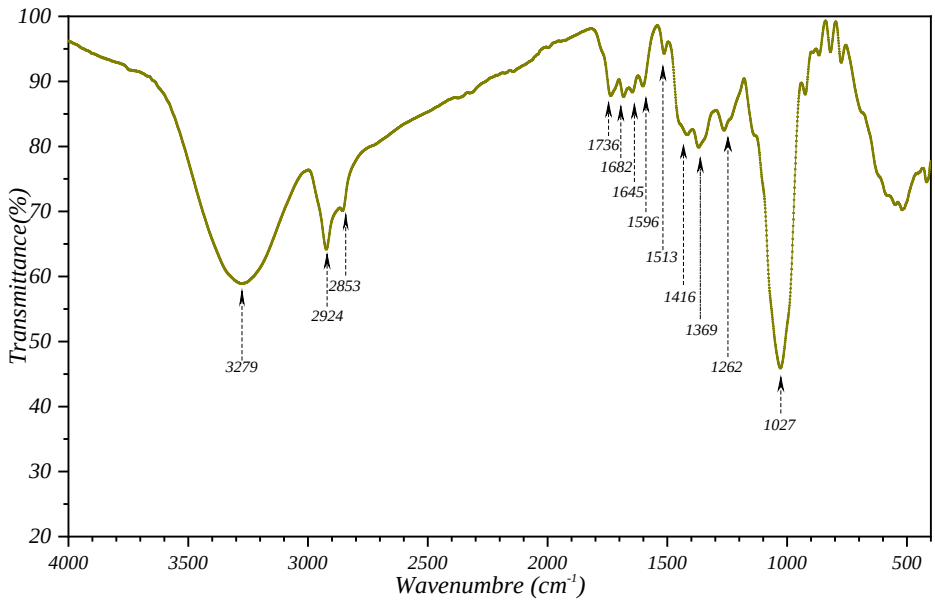


**Figure 1:** FTIR spectra of CTE.

**Table 1:** CR variations of CS samples dependent on concentration in 1M HCl at 298 K during 6 hours.

| C (g/L) | Δm (mg/cm$^2$) | CR (mg cm$^{-2}$ h$^{-1}$) | Inhibition Efficiency (%) |
|---|---|---|---|
| 0 | 48.24 | 0.67 | ------- |
| 0.5 | 14.40 | 0.20 | 70 |
| 1 | 12.24 | 0.17 | 75 |
| 2 | 10.08 | 0.14 | 79 |
| 2.5 | 07.20 | 0.10 | 85 |

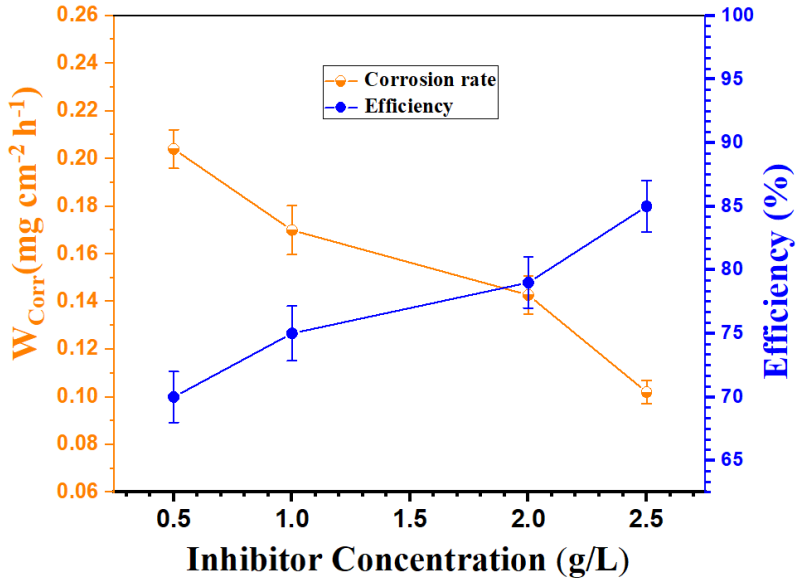


**Figure 2:** CTE concentration effects on CS weight loss in 1M HCl (298 °K).

The investigations were further conducted under four discrete temperature conditions (298, 308, 318, and 338 °K) using an extract concentration of 2.5 g/L. As demonstrated in Figure 3a, both temperatures had an influence on the results. At the critical concentration of 2.5 g/L, the inhibition efficiency decreased from 85 % at 298 K to 68 % at 338 K, resulting from the rapid deterioration caused by corrosion at higher temperatures, which reflects that the extract's efficacy is influenced by temperature [31].

Figure 3b shows how the inhibition efficiency changed over time at the optimum of 2.5 g/L. The data reveal a reduction in inhibition efficiency during the initial period (from 30 minutes to 2 hours), followed by a gradual increase in IE (%), which stabilizes at 85 %. The impact of immersion time, considering the seven durations examined, revealed a small difference in IE (%) values, spanning only 4 %. This suggests that this Cistanche tubulosa (CT) extract can effectively inhibit CS corrosion in hydrochloric acid solutions, even with extended immersion.

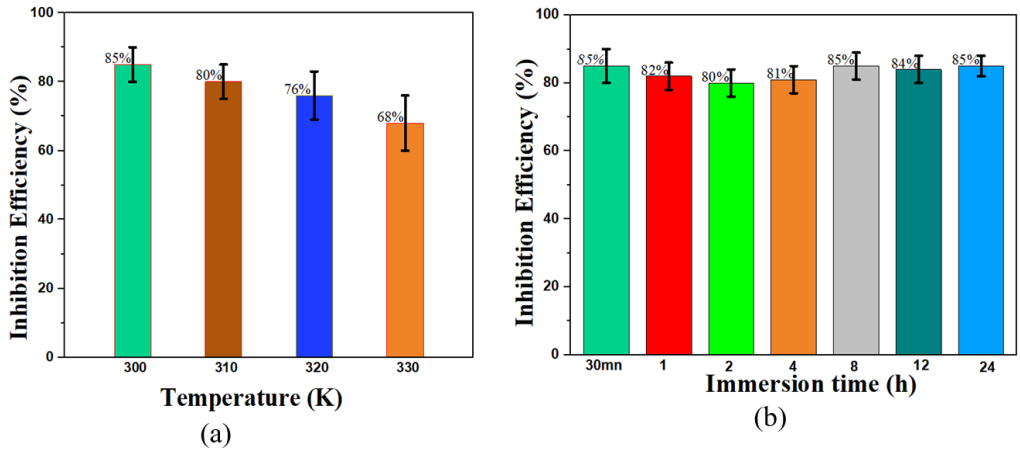


**Figure 3:** Effect of temperature (a) and immersion time (b) on the inhibition efficiency of 2.5 g/L CTE concentration towards CS corrosion across 1 M HCl.

### 3.3. Inhibition effect study

#### 3.3.1. Open circuit potential

In free corrosion conditions, the OCP of CS immersed in a 1M HCl medium was measured over time until a stable potential state (Figure 4 at 298 °K). Without CTE, the potential increases for 1800 seconds and then becomes stable. This could result from the formation of a protective film, leading to surface passivation. Upon the addition of the inhibitor, the electrode potential achieves a state of dynamic equilibrium at 480 mV vs. ECS at an inhibitor concentration of 2.5 g/L CT. This variation is attributable to the interface modification, and a stable state is reached after 30 minutes. This was when EIS and PDP measurements were executed.

#### 3.3.2. Electrochemical polarization

Figure 5 displays the electrochemical polarization curves of the electrode soaked for 30 minutes in 1 M HCl, with varying concentrations of CTE inhibitor applied. As shown in Figure 5, the introduction of CTE into the HCl (1 M) results in a notable diminution of current densities as compared to the uninhibited electrolyte, with this effect being markedly more in the anodic than in the cathodic branch. At the cathode, the curves run parallel, revealing that the cathodic mechanism (hydrogen reduction: $2H^+ + 2e^- \rightarrow H_2$) [32] is unaffected by the inhibitor [33]. Conversely, in the anodic branch, introducing the inhibitor leads to a significant change in the curve, suggesting an alteration in the anodic reaction mechanism (metal dissolution: $Fe \rightarrow Fe^{2+} + 2e^-$) [34].

In the anodic branch, a notable change in slope was observed between the corrosion potential of -400 mV/ECS and -320 mV/ECS. Beyond this region, a notable increment in current density was observed, indicative of the desorption of inhibitors from the electrode surface [35]. This phenomenon, known as desorption, is characterized by a desorption potential of -300 mV/ECS.

The corrosion potential exhibited negligible variation with the inhibitor included. Potential deviations from the reference were ≤ 85 mV across inhibitor concentrations, indicating that the inhibition mechanism type is mixed, with anodic predominance [36]. The parameters corrosion potential, Tafel slopes, and current densities were calculated and are listed in Table 2, The performance of the inhibitor, denoted as η%, was determined using the following equation 3 [37]:

$$\eta\% = \frac{i_{corr,0} - i_{corr}}{i_{corr,0}} \times 100 \qquad (3)$$

Table 2 shows a decrease in $I_{corr}$ with the addition of CTE vis-à-vis the blank, with the current density decreasing from 174.4 µA/cm² to 14.82 µA/cm² with the addition of 2.5 g/L of CT extract. Inhibition efficiency increases proportionally to the inhibitor concentration, reaching a peak of 92 % at a concentration of 2.5 g/L.

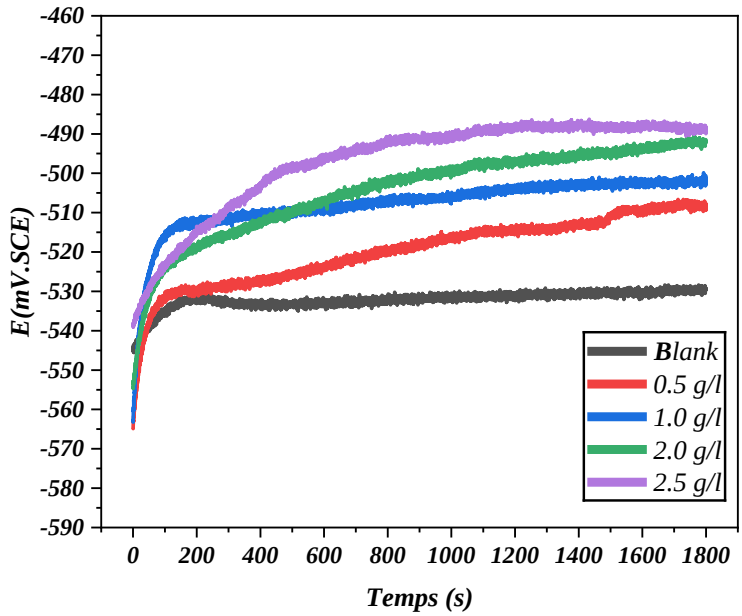


**Figure 4:** The OCP curves of CS in a 1.0 mol/L HCl with and without CTE inhibitor at 298 K.

**Table 2:** The parameters of a CS electrode dipped in a 1.0 M HCl at 298 K, obtained from the PDP curves.

| C (g/L) | | -$E_{corr}$ (mV/SCE) | $I_{corr}$ (µA.cm$^{-2}$) | βc (mV.dec$^{-1}$) | βa (mV.dec$^{-1}$ ) | |
|---|---|---|---|---|---|---|
| CT | 0 | 525.7 | 174.4 | 58.6 | 88.6 | ---------- |
| | 0.5 | 494 | 31.4 | 56 | 64 | 82 |
| | 1 | 490 | 24.42 | 51 | 62.4 | 86 |
| | 2 | 478 | 19.18 | 52 | 62.8 | 89 |
| | 2.5 | 477 | 14.82 | 49 | 61 | 92 |

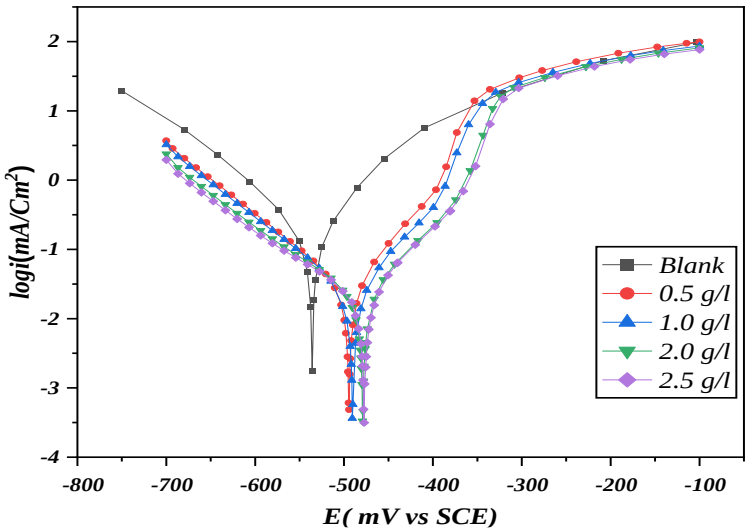


**Figure 5:** The electrochemical polarization curves of the CS with and without CTE at 298 °K.

These results demonstrate the inhibitor's good protection of the electrode surface against aggressive attacks; this is likely a result of CTE molecules being adsorbed [38]. The high level of inhibition is associated with the presence of donor and acceptor sites within the molecular structure of the inhibitor [39].

To better contextualize the efficiency of the Cistanche tubulosa extract compared to other reported inhibitors in the literature, Table 3 presents a comparison of inhibition performance under similar conditions. This comparison highlights the remarkable efficiency of the studied extract, particularly in terms of reduced corrosion current density and high inhibition efficiency (IE%). EIS tests were carried out for a more detailed study.

### 3.3.3. Electrochemical impedance characterization

Figure 6 visualizes the Nyquist diagrams of CS immersed in a 1 M HCl solution, with and without the introduction of extract at different concentrations. The observed impedance spectra don't exhibit the perfect semicircular shape. This deviation from the ideal form can result from the dispersion of the interfacial impedance as a function of frequency. This dispersion is related to the heterogeneity of the electrode surface, which can originate from various factors, such as roughness, the presence of impurities, and the deposition of the inhibitor, resulting in the formation of a porous layer [43].

**Table 3:** Comparison of the inhibition efficiency of CTE with other reported inhibitors under similar conditions.

| Inhibitor | Metal | Medium | $I_{corr}$ (µA.cm$^{-2}$) | EI% | Ref. |
|---|---|---|---|---|---|
| Cistanche tibulusa | Carbon steel | 1.0 HCl | 14.82 | 92 | This study |
| Moringa peregrina | Carbon steel | 1.0 HCl | 43.30 | 78.6 | [40] |
| Acriflavine | Mild steel | 1.0 HCl | 81.3 | 92 | [41] |
| Chinese gooseberry | Mild steel | 1.0 HCl | 91 | 85.37 | [42] |

Each of these diagrams presents a deformed capacitive loop. The loop's area expands with higher extract concentrations, as confirmed by the increase in polarization resistance. Figure 7 presents the electrical analogue used to simulate the EIS data. Table 4 summarizes the electrochemical parameter values and the EI% determined by EIS for different concentrations of the CT extract. Inhibition efficiency can be expressed in a multiplicity of ways, the prevailing expression defined by the following equation 4 [44]:

$$\eta\,\% = \frac{R_{P,Inh} - R_{P,Blank}}{R_{P,Inh}} \times 100 \qquad (4)$$

where $R_{P,inh}$ and $R_{P,blank}$ are the charge transfer impedance of CS after immersion with and free from of the CTE, respectively.

EIS parameters (Table 4) were utilized to evaluate the effectiveness of corrosion inhibitors for protecting CS electrodes dipped in HCl (1.0 M) at 298 °K. According to the table data, the increase in Rp indicates the performance of the extract against corrosion, which is already confirmed through the diminution of $i_{corr}$. The act of raising inhibitor concentration leads to a decline in Cdc. This reduction is attributed to the adsorption of inhibitor molecules onto the CS surface, which creates a protective barrier that hinders charge transfer at the metal-solution interface [45]. Indeed, the more the extract adsorbs onto the CS surface, the thicker the protective layer formed becomes, which further decreases the capacitance of the electrical double layer. The concor-dance of the results obtained by EIS and PDP tests attests to the reliability and consistency of the data on the corrosive properties of the extract.

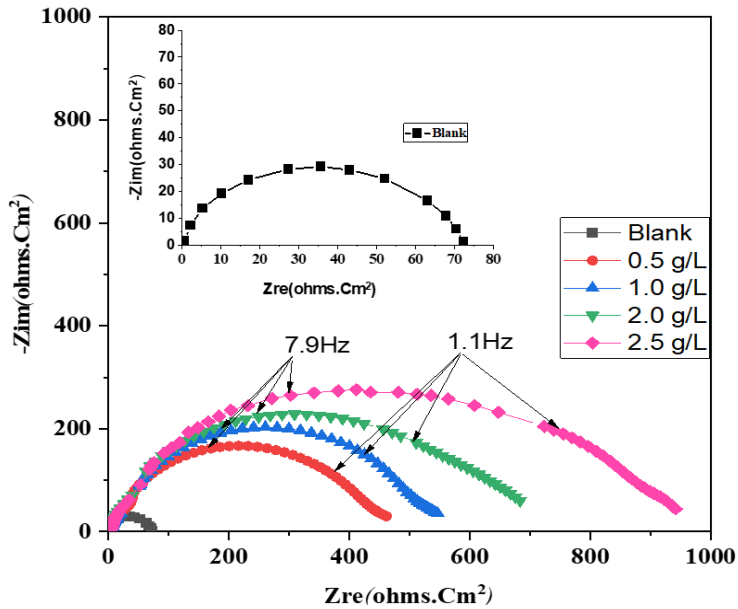


**Figure 6:** EIS of CS in 1M HCl Solution with varying concentrations of CTE at 298 °K.

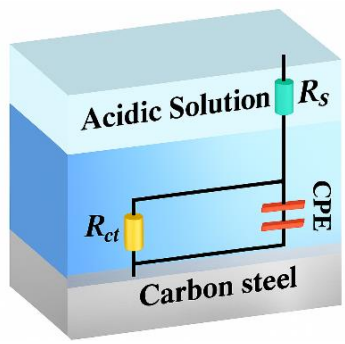


**Figure 7:** The adopted circuit model.

**Table 4:** EIS parameters were utilized to evaluate the effectiveness of corrosion inhibitors for protecting CS electrodes dipped in HCl (1.0 M) at 298 °K.

| C (g/L) | | Rs (Ω/cm²) | Rct (Ω/cm²) | Cdl (µf/cm²) | n | Qdl | Ŋ (%) |
|---|---|---|---|---|---|---|---|
| CT | 0 | 0.62 | 73.78 | 211.3 | 0.88 | 340 | ---- |
| | 0.5 | 1.02 | 461.00 | 100.0 | 0.76 | 120 | 84 |
| | 1.0 | 2.30 | 546.00 | 87.0 | 0.91 | 99 | 87 |
| | 2.0 | 2.70 | 683.00 | 45.0 | 0.83 | 43 | 89 |
| | 2.5 | 2.83 | 941.00 | 21.0 | 0.86 | 37 | 92 |

### 3.4. The temperature variation effects

To understand the Temperature's impact on steel in a corrosive environment, similar tests were conducted in a 1 M hydrochloric acid solution, both 0 and 2.5 g/L of CTE, at a selection of temperatures. Polarization measurements were conducted to examine the corrosion-resistant effectiveness of CTE at 298, 308, and 318 K. Figure 8 illustrates the Tafel polarization curves of working electrodes (CS) immersed in 1.0M HCl media containing 0 and 2.5 g/L CTE at various temperatures. Relevant experimental parameters are summarized in Table 5.

The information conveyed in Figure 8a indicates that the curves for both the anodic and cathodic regions are approximately parallel, suggesting that temperature does not alter the fundamental anodic and cathodic reactions, but rather influences their reaction rates. However, in a solution containing the inhibitor (Figure 8b), the curves remain roughly parallel in the cathodic region but not in the anodic region. This suggests that, when the inhibitor is present, temperature influences both the anodic corrosion mechanism and the intensity of corrosion [46].

As the temperature increased, both the reference solution and inhibited solutions exhibited alterations in the PDP plots, shifting toward higher corrosion current densities, which led to an increase in the icorr value. This trend indicates that the corrosion rate of CS accelerates with rising temperature, likely due to enhanced thermal agitation of CT molecules, which destabilizes the adsorption layer and accelerates corrosion.

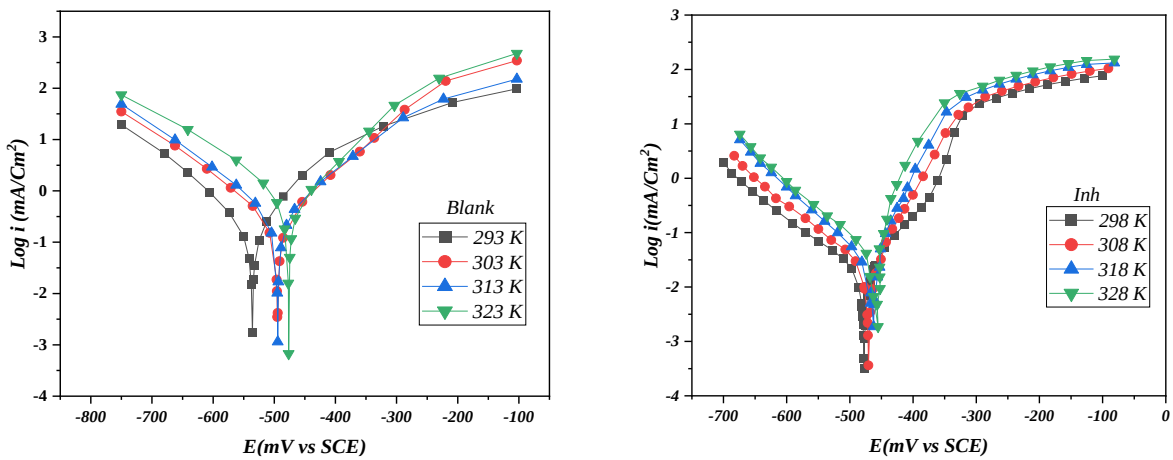


(a) (b)

**Figure 8:** The PDP plots of CS in 1M HCl w/o 2.5g/L at different temperatures.

**Table 5:** Electrochemical parameters are measured for CS electrodes in 1.0 M HCl solution at various T, with and without the presence of 2.5 g/L CTE concentrations.

| T (K) | C (g/L) | -$E_{corr}$ (mV/SCE) | $I_{corr}$ (µA/cm$^2$) | Bc (mV/dec$^1$) | βa (mV/dec$^1$ ) | Ƞ (%) |
|---|---|---|---|---|---|---|
| 298 | 0 | 525.7 | 174.4 | 58.6 | 88.6 | |
| | 2.5 | 477 | 14.82 | 49 | 61 | 92 |
| 308 | 0 | 494.7 | 269.04 | 96.8 | 115.5 | |
| | 2.5 | 459 | 34.97 | 63 | 71 | 87 |
| 318 | 0 | 494.5 | 373.61 | 110.2 | 121.4 | |
| | 2.5 | 436 | 63.51 | 69 | 83 | 83 |
| 328 | 0 | 476.51 | 595.89 | 93.1 | 114.1 | |
| | 2.5 | 415 | 119.16 | 72 | 88 | 80 |

In opposition to the reference solution, the inclusion of 2.5 g/L CTE at each discrete temperature significantly reduced the icorr value, indicating effective inhibition of CS corrosion. However, the protective quality of the CT adsorption film weakened with increasing temperature, as evidenced by the decrease in the EI % from 92 % at 298 °K to 80 % at 328 °K. Despite the accelerating effect of temperature on corrosion, CT still demonstrated excellent inhibition performance at 328 °K.

### 3.5. Immersion time's effect on inhibition

To test the quality of CTE and the surface film created on the CS, the Rct was measured at discrete immersion times (0.5, 1, 2, 4, 8, 10, 12, 24 h) in a 1M HCl solution, containing and lacking 2.5 g/L of CTE at 298K. The results, presented in the form of electrochemical impedance diagrams (Figure 9), enabled the extraction of electrochemical corrosion parameters, which are detailed in Table 6.

After a 30-minute immersion, a slight decrease in the interfacial reaction impedance values is observed**.** The mechanism behind this phenomenon is the desorption of protective molecules from the CS surface, resulting from conditions associated with increased surface roughness during exposure [47].

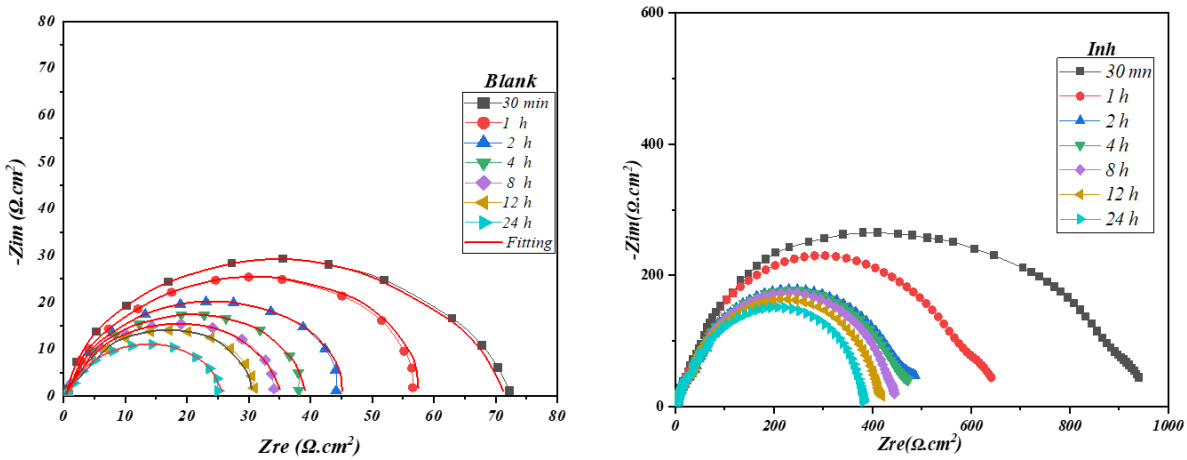


(a) (b)

**Figure 9:** EIS Nyquist plots of CS for a) 1 M HCl and b) 1 M HCl + 2.5 g/L CTE, with varied immersion durations, at 298 °K.

**Table 6:** CS electrochemical parameters changes with immersion time in 1.0 M HCl containing 2.5 g/L CT extract, at 298 °K.

| Medium | Immersion time | Rs ($\Omega/cm^2$) | Rct ($\Omega/cm^2$) | Cdl($\mu F/cm^2$) | n | Qdl ($\mu\omega^1/cm^2.Sn$) | IE (%) |
|---|---|---|---|---|---|---|---|
| HCl (1M) | 30 min | 0.62 | 73.78 | 211.3 | 0.88 | 340 | ------ |
| | 1h | 0.20 | 57.86 | 118.6 | 0.84 | 247.6 | ------ |
| | 2h | 0.95 | 45.99 | 261 | 0.92 | 363.4 | ----- |
| | 4h | 1.06 | 39.91 | 365.2 | 0.96 | 425.9 | ------- |
| | 8h | 0.69 | 35.64 | 472.5 | 0.91 | 669.6 | ------ |
| | 12h | 0.552 | 31.6 | 760.8 | 0.89 | 1110 | ------ |
| | 24h | 0.543 | 27.36 | 1510 | 0.87 | 2301 | ------- |
| CT (2.5g/L) | 30 mn | 2.83 | 941 | 21 | 0.86 | 37 | 92 |
| | 1h | 3.06 | 644 | 23 | 0.8 | 36.7 | 91 |
| | 2h | 5.8 | 490 | 32 | 0.86 | 40.6 | 91 |
| | 4h | 1 | 470 | 25 | 0.79 | 41.1 | 91 |
| | 8h | 0.9 | 444 | 28 | 0.81 | 44.3 | 92 |
| | 12h | 1 | 418 | 28 | 0.9 | 50.4 | 92 |
| | 24h | 2 | 380 | 29 | 0.87 | 49.8 | 92 |

Subsequently, the charge transfer resistance values remain stable and equal to the initial measurement. The results obtained corroborate the durability of the inhibiting layer, indicating that CTE is effective for protecting CS from corrosion in hydrochloric media even at long immersion times.

## 3.6. Adsorption isotherms

The effectiveness of a corrosion inhibitor largely depends on its ability to adsorb onto the metal surface. Adsorption isotherms are essential tools for analyzing this process, as they offer insight into the interactions between adsorbed species and the metal surface, as well as among the adsorbed particles themselves. Understanding the adsorption mechanism is therefore crucial, as it reveals key aspects of the reactivity between the inhibitor and the metal substrate [48]. To identify the most appropriate adsorption isotherm, several models, including the Langmuir, Freundlich, and Flory–Huggins adsorption isotherms, were investigated. These isotherms show the relationship between the inhibitor concentration ($C_{inh}$) and adsorption, and are described by the following equations in Table 7. Figure 10 shows the set of isotherms obtained for the extract CT in 1 M HCl solution. For each plot, a linear regression analysis was performed using the corresponding data.

**Table 7:** Summary of adsorption isotherm models applied in corrosion inhibition studies.

| Isotherm model | Linear equation | Descriptions | Ref. |
|---|---|---|---|
| Langmuir | $\frac{C}{q} = \frac{1}{q_{max}k_L} + \frac{C}{q_{max}}$ | C: The inhibitor concentration<br>$q_{max}$: The maximum adsorption capacity (mg/g)<br>$K_L$: The Langmuir constant (L/mg) | [49] |
| Freundlich | $log\theta = logk_F + \left(\frac{1}{n}\right).logC$ | $K_F$: Freundlich constant (L/mg)<br>1/n: adsorption intensity | [50] |
| Flory–Huggins | $\log\left(\frac{\theta}{C}\right) = logk_{FH} + n.log(1-\theta)$ | $K_{FH}$: Flory–Huggins constant (L/mg)<br>n: adsorption intensity(J/mol) | [51] |

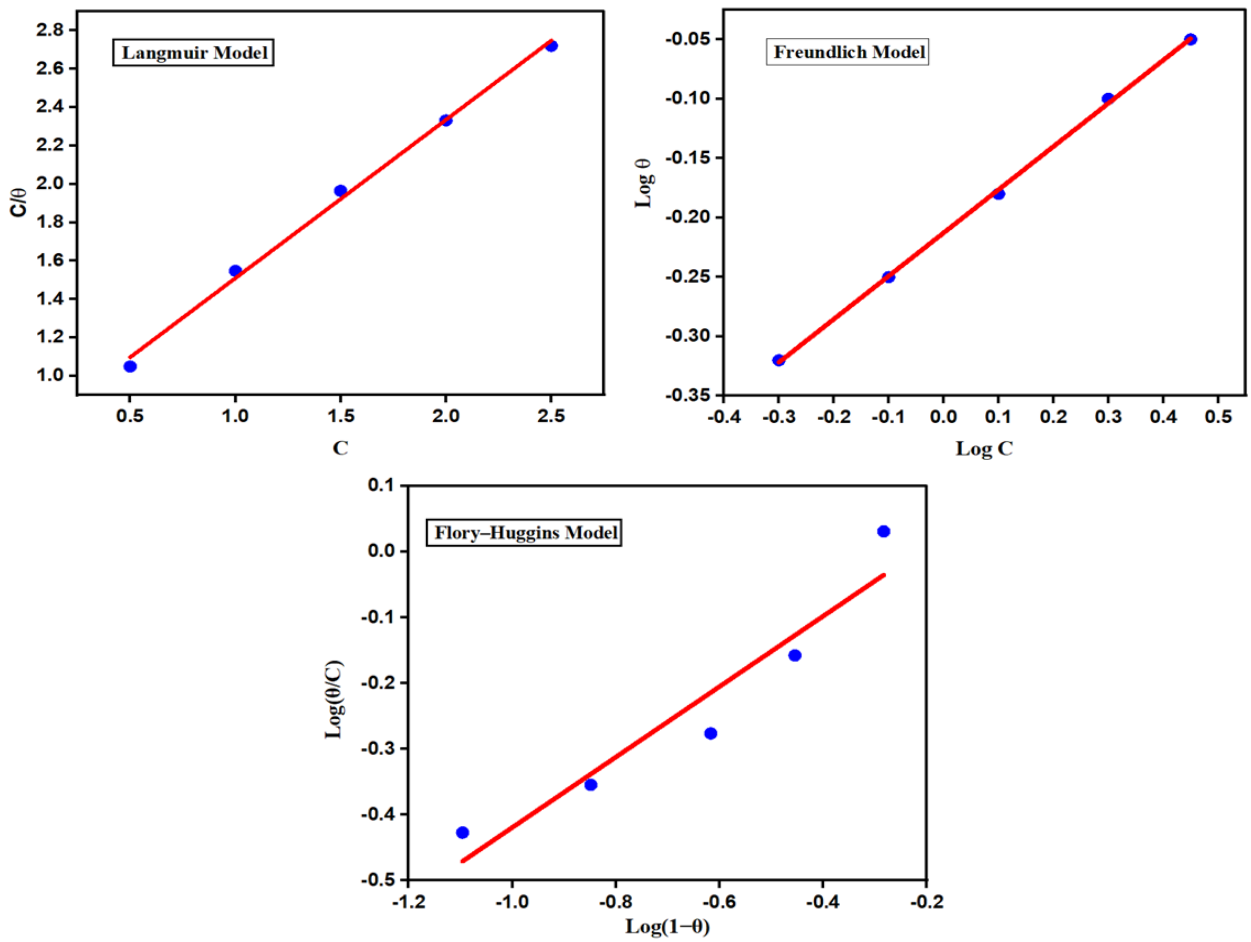


**Figure 10:** Adsorption isotherms using CTE for CS in 1 M HCl at 298 °K.

Table 8 presents the parameters of the Langmuir, Freundlich, and Flory–Huggins isotherm models, obtained by fitting the experimental data, along with their coefficients of determination ($R^2$).

The interpretation of the isotherm data presented in Table 8 and Figure 10 reveals significant insights into the adsorption behavior of CTE. According to the Langmuir model, $\Theta_{max}$, is 1.208 mg/g, with an adsorption constant $K_L$ of 1.221 L/mg, and a high correlation coefficient ($R^2$ = 0.99566), reflecting a well-fitted monolayer adsorption on a homogeneous surface. The high $K_L$ value indicates a strong affinity between inhibitor molecules and the metal surface, suggesting a predominantly chemisorption process.

In contrast, the Freundlich model shows an excellent statistical fit ($R^2$ = 0.99814), demonstrating strong agreement with the experimental data. However, the Freundlich constant n = 0.48089 (< 1) indicates unfavorable energetic conditions for adsorption, often associated with multilayer formation on a heterogeneous surface.

**Table 8:** The parameters of the Langmuir, Freundlich, and Flory–Huggins isotherm models.

| Isotherm | Langmuir | | | Freundlich | | | Flory-Huggins | | |
|---|---|---|---|---|---|---|---|---|---|
| **Parameters** | $q_m$ (mg/g) | $K_L$ (L/mg) | $R^2$ | $K_F$ (L/mg) | n | $R^2$ | $K_{FH}$ (L/mg) | n | $R^2$ |
| **values** | 1.208 | 1.221 | 0.99566 | 0.642 | 0.48089 | 0.99814 | 1.154 | 0.48715 | 0.91773 |

Despite the strong statistical fit, the physical interpretation suggests limited surface coverage at higher concentrations. The Flory–Huggins isotherm further supports the physical nature of the interaction, with a correlation coefficient of $R^2 = 0.91773$ and a value of $n = 0.48715$, indicating that each inhibitor molecule displaces less than a water molecule. This suggests a relatively weak, predominantly electrostatic adsorption process.

Overall, while the Freundlich model shows the best statistical fit, the Langmuir model offers a more realistic representation of the adsorption mechanism, emphasizing strong specific interactions at well-defined sites. The Flory–Huggins analysis confirms the partial physical character of the inhibitor's adsorption on the metal surface.

### 3.7. SEM surface morphology analysis

SEM imaging was conducted at 298 K to determine the CS morphology with and without CTE in a 1.0 M HCl solution. The CS sample had dimensions of 30 × 30 × 20 mm. A visual display of the findings is provided in Figure 11. Figure 11a illustrates the surface of the polished steel before exposure to the corrosive solution, where distinct parallel lines, associated with abrasion marks from the polishing process, are observable. Figure 11b shows a CS sample immersed in a 1M HCl for 24 hours at 298 °K. The CS surface appears rough and irregular. Indicating significant CS corrosion in the uninhibited solution. Figure 11c shows the CS surface immersed in a 1M hydrochloric acid solution with a corrosion inhibitor (CT). The addition of CT extract results in a visibly smoother CS surface effectively suppressing sample corrosion. This observation suggests that a CTE adsorption layer is generated on the CS surface.

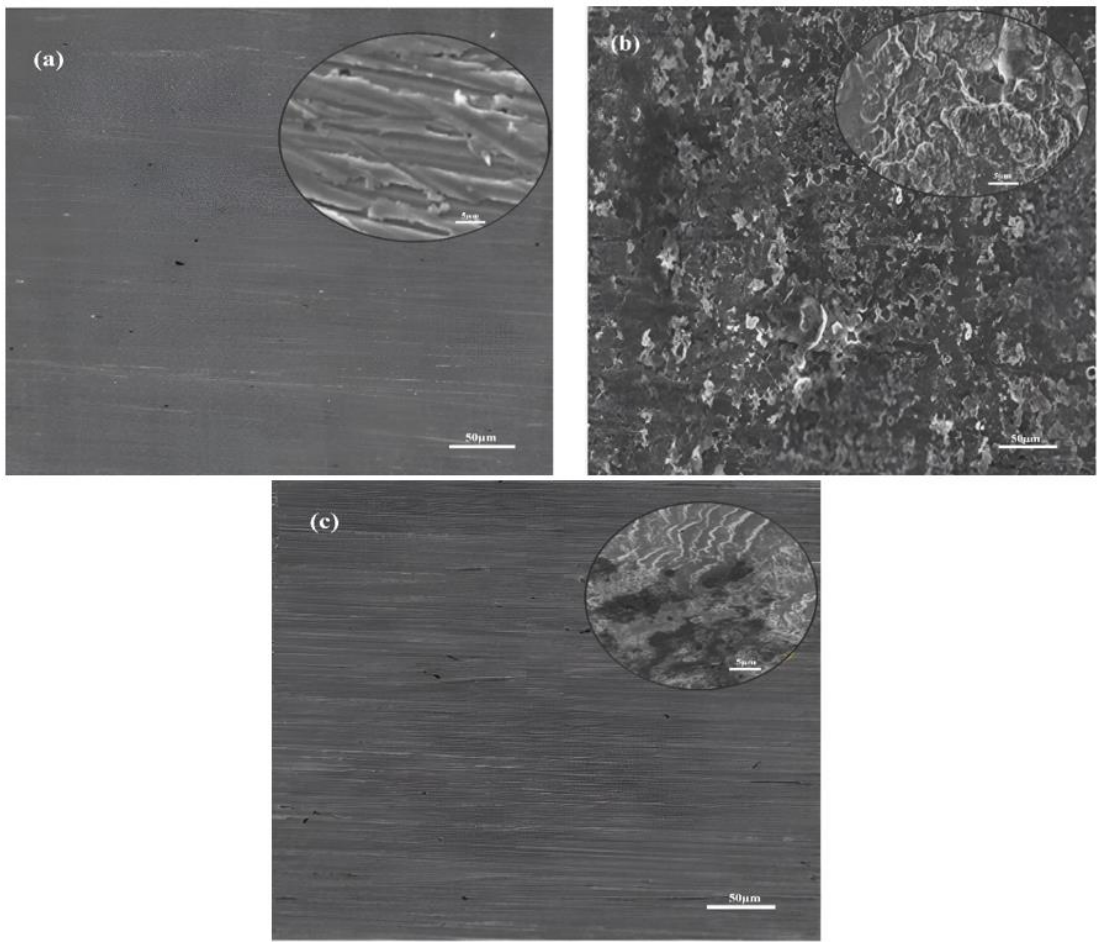


**Figure 11:** SEM images of carbon steel (a) polished only, (b) exposed to HCl, (c) exposed to HCl + 2.5 g/L CTE.

## 4. Conclusion

Gravimetric, electrochemical, and surface analytical methods were employed to assess the inhibitory capacity of Cistanche tubulosa. The CTE contains several functional groups deployed as a biodegradable inhibitor for CS in 1.0 M HCl medium. The mass loss method indicates that Cistanche tubulosa is suitable as a natural inhibitor in acidic medium at low concentrations, high temperature, and prolonged immersion time. The Tafel polarization technique demonstrated a maximum inhibition efficacy of 92 % in 1.0 M HCl with 2.5 g/L CTE at a temperature of 298 K. The CT extract acts as a mixed-type corrosion inhibitor, and its adsorption behavior follows the Langmuir isotherm model. The adsorption of its phytochemical constituents onto the metal surface occurs primarily through chemisorption. Although a decrease in inhibition efficiency was observed with increasing temperature (80 % at 328 °K), this reduction remains moderate, suggesting that CTE still offers considerable protection at higher temperatures. Therefore, while temperature does affect inhibition performance, the extract maintains acceptable efficacy, confirming its potential as a practical corrosion inhibitor under varying thermal conditions. EIS testing confirmed that as immersion time increased. Surface coverage improved, and high inhibitor efficiency was maintained. The surface morphology analysis reveals that the degradation of CS is greatly limited by the adsorption of CTE components on the surface, forming a protective film, which manifests the protective action of CTE in 1.0 M HCl. There is good agreement between the findings achieved by the three techniques. It can be concluded that the CT extract is an effective, economical, and good plant-based inhibitor for limiting corrosion on the CS surface in HCl medium.

## 5. References


1. Tan B, Zhang S, Liu H, Guo Y, Qiang Y, Li W, et al. Corrosion inhibition of X65 steel in sulfuric acid by two food flavorants 2-isobutylthiazole and 1-(1.3-Thiazol-2-yl) ethanone as the green environmental corrosion inhibitors: combination of experimental and theoretical researches. J Colloid Interface Sci. 2019;538:519-29. https://doi.org/10.1016/j.jcis.2018. 12. 020.
2. Li H, Qiang Y, Zhao W, Zhang S. A green Brassica oleracea L extract as a novel corrosion inhibitor for Q235 steel in two typical acid media. Colloids Surf A Physicochem Eng Asp. 2021;616:126077. https://doi. org/10.1016/j.colsurfa.2020.126077.
3. Tan B, Xiang B, Zhang S, Qiang Y, Xu L, Chen S, et al. Papaya leaves extract as a novel eco-friendly corrosion inhibitor for Cu in $H_2SO_4$ medium. J Colloid Interface Sci. 2021; 582:918-31. https://doi.org/10. 1016/ j.jcis.2020.08.093.
4. Ding J, Zhao H, Zhao X, Xu B, Yu H. How semiconductor transition metal dichalcogenides replaced graphene for enhancing anticorrosion. J Mater Chem A. 2019;7(22):13511-21. https://doi.org/ 10. 1039/C9TA04033A.
5. Zhang G, Wu L, Tang A, Ma Y, Song GL, Zheng D, et al. Active corrosion protection by a smart coating based on a MgAl-layered double hydroxide on a cerium-modified plasma electrolytic oxidation coating on Mg alloy AZ31. Corros Sci. 2018; 139:370-82. https://doi.org/10.1016/j.corsci.2018.05.010.
6. Liao LL, Mo S, Luo HQ, Li NB. Corrosion protection for mild steel by extract from the waste of lychee fruit in HCl solution: experimental and theoretical studies. J Colloid Interface Sci. 2018; 520:41-9. https://doi.org/10.1016/j.jcis.2018.02.071.
7. Chraka A, Seddik NB, Raissouni I, Kassout J, Choukairi M, Ezzaki M, et al. Electrochemical explorations, SEM/EDX analysis, and quantum mechanics/molecular simulations studies of sustainable corrosion inhibitors on the Cu-Zn alloy in 3% NaCl solution. J Mol Liq. 2023; 387:122715. https://doi.org/10.1016/j.molliq.2023.122715.
8. Asadi N, Ramezanzadeh M, Bahlakeh G, Ramezanzadeh B. Utilizing Lemon Balm extract as an effective green corrosion inhibitor for mild steel in 1 M HCl solution: a detailed experimental, molecular dynamics, Monte Carlo and quantum mechanics study. J Taiwan Inst Chem Eng. 2019; 95:252-72. https://doi.org/10.1016/j.jtice.2018.07.011.
9. Liao LL, Mo S, Luo HQ, Li NB. Longan seed and peel as environmentally friendly corrosion inhibitor for mild steel in acid solution: experimental and theoretical studies. J Colloid Interface Sci. 2017; 499:110-9. https://doi.org/10.1016/j.jcis.2017.03.091.
10. El-Hashemy MA, Sallam A. The inhibitive action of Calendula officinalis flower heads extracts mild steel corrosion in 1 M HCl solution. J Mater Res Technol. 2020; 9(6):13509-23. https://doi.org/10.1016/j.jmrt. 2020.09.078.
11. Lavanya M, Suvarna AS, Kumari PP. Adsorption and corrosion inhibition behaviour of Pterocarpus marsupium stem extract on mild steel in acid medium: experimental and statistical approach. Can Metall Q. 2024;63(4):1335-46. https://doi.org/10.1080/000844 33. 023.2273705.

12. Pahuja P, et al. An eco-friendly corrosion inhibitor Cuscuta reflexa extract and PEG400 for mild steel inhibition in acidic medium: computational and experimental investigations. Environ Sci Pollut Res. 2023;30(44):98701-17. https://doi.org/10.1007/s11356-022-23842-8.
13. Doumane G, et al. Corrosion inhibition performance of Citrullus colocynthis seed oil extract as a mild steel in 1.0 M HCl acid using various solvents such as petroleum ether (CSOP) and cyclohexan (CSOC) polymerics. Inorg Chem Commun. 2023; 155:111042. https://doi.org/10.1016/j.inoche.2023.111042.
14. Berrissoul A, et al. Experimental and theoretical insights into Artemisia stems aqueous extract as a sustainable and eco–friendly corrosion inhibitor for mild steel in 1 M HCl environment. Environ Sci Pollut Res. 2024;31(25):36643–62. https://doi.org/10.1007/s11356-024-33636-9.
15. Kotupalli MR, Sahini MG, Pulapa VKR, Elisadiki J. Corrosion inhibition of mild steel by Plumeria rubra flower extract: electrochemical and computational study. Chemistry Select. 2024; 9(46):e202403617. https://doi.org/10.1002/slct.202403617.
16. Ezugha SI, Aralu CC, Eze VC. Inhibition potentials of Solanum macrocarpon leaf extract as a green corrosion inhibitor of mild steel in an acidic solution. J Bio-Tribo-Corros. 2024; 10:81. https://doi.org/10.1007/s40735-024-00885-7.
17. Ezzat AO, Aigbodion VS, Al-Lohedan HA, Ozoude CJ. Unveiling the corrosion inhibition efficacy and stability of silver nanoparticles synthesized using Anacardium occidentale leaf extract for mild steel in a simulated seawater solution. RSC Adv. 2024; 14(26):18395-405. https://doi.org/10.1039/D4RA02362E.
18. Morikawa T, Xie H, Pan Y, Ninomiya Y, Matsuda H, Yoshikawa M. A review of biologically active natural products from a desert plant Cistanche tubulosa. Chem Pharm Bull. 2019;67(7):675-89. https://doi:10.1248/cpb.c19-00008.
19. Liu X, Yan Y, Liu Y, Yuan H, Luo Y, Yang B. Cell culture establishment and regulation of two phenylethanoid glycosides accumulation in cell suspension culture of desert plant Cistanche tubulosa. Plant Cell Tissue Organ Cult. 2018; 134:107–18. https://doi.org/10.1007/s11240-018-1404-y.
20. Al-Snafi AE. Bioactive metabolites and pharmacology of Cistanche tubulosa-A review. IOSR J Pharm. 2020; 10(1):37-46. https://doi.org/10.1007/s11240-018-1404y.
21. Khodjamkulov SZ, Kh MZ. Salsola Oppositifolia acid extract as a green corrosion inhibitor for carbon steel. Indian J Chem Technol. 2023;30(6):872–7. https://doi:10.56042/ijct.v30i6.6553.
22. Modwi MMY, Feng H, Hadi MK, Chen N, Hou J, Kamal E, et al. Eco-friendly corrosion inhibitor of Q235 carbon steel in 1.0 M HCl by Isatin/Chitosan Schiff base. J Mol Struct. 2025; 1321:139592. https://doi.org/10.1016/j.molstruc.2024.139592.
23. Wu Y, Guo L, She Y. Insight on the corrosion inhibition performance of Psidium guajava Linn leaves extract. J Mol Liq. 2022;346:117858. https://doi.org/10.1016/j.molliq.2021.117858.
24. Ghazoui M, Elkacmi R, Sylla AS, Moulakhnif K, Touzani I, Boudouch O. Efficient removal of methylene blue and methyl red dyes using a novel adsorbent derived from Saponaria officinalis root via $H_3PO_4$, $H_2SO_4$, and KOH-activation: optimization, kinetics, and isotherm study. Desalin Water Treat. 2024;318:100378. https://doi.org/10.1016/j.dwt. 2024. 100378.
25. Ghazoui M, Elkacmi R, Sylla AS, Moulakhnif K, Touzani I, Boudouch O. Assessment of Rhus pentaphylla-sulfuric acid activated carbon performance for cadmium ions adsorption: mechanism, response surface methodology optimisation, and cost estimation. Indian Chem Eng. 2025 Feb. https://doi.org/10.1080/00194506.2025. 2462953.
26. Kareem MO, Edathil AA, Rambabu K, Bharath G, Banat F, Nirmala G, Sathiyanarayanan K. Extraction, characterization and optimization of high quality bio-oil derived from waste date seeds. Chem Eng Commun. 2021; 208:801-11. https://doi.org/10.1080/00986445.2019.1650034.
27. Sanaei Z, Ramezanzadeh M, Bahlakeh G, Ramezanzadeh B. Use of Rosa canina fruit extract as a green corrosion inhibitor for mild steel in 1 M HCl solution: a complementary experimental, molecular dynamics and quantum mechanics investigation. J Ind Eng Chem. 2019; 69:18-31. https://doi.org/10.1016/j.jiec.2018.09.013.
28. Qiang Y, Zhang S, Tan B, Chen S. Evaluation of Ginkgo leaf extract as an ecofriendly corrosion inhibitor of X70 steel in HCl solution. Corros Sci. 2018; 133:6-16. https://doi.org/10.1016/j.corsci. 2018. 01.008.
29. Habibiyan A, Ramezanzadeh B, Mahdavian M, Kasaeian M. Facile size and chemistry-controlled synthesis of mussel-inspired bio-polymers based on polydopamine nanospheres: application as eco-friendly corrosion inhibitors for mild steel against aqueous acidic solution. J Mol Liq. 2020; 298:111974. https://doi.org/10.1016/j.molliq.2019.111974.
30. Cherrad S, Alrashdi AA, Lee HS, Lgaz H, Satrani B, Ghanmi M, et al. Cupressus arizonica fruit essential oil: a novel green inhibitor for acid corrosion of carbon steel. Arab J Chem. 2022; 15(6):103849. https://doi.org/10.1016/j.arabjc.2022.103849.
31. Liu FG, Du M, Zhang J, Qiu M. Electrochemical behavior of Q235 steel in saltwater saturated with carbon dioxide based on new imidazoline derivative inhibitor. Corros Sci. 2009;51(1):102-9. https://doi.org/10.1016/j.corsci.2008.09.036.
32. Haruna K, Obot IB, Ankah NK, Sorour AA, Saleh TA. Gelatin: A green corrosion inhibitor for carbon steel in oil well acidizing environment. J Mol Liq. 2018; 264:515-525. https://doi.org/10.1016/j.molliq. 2018.05.058

33. Dehghani A, Bahlakeh G, Ramezanzadeh B. A detailed electrochemical/theoretical exploration of the aqueous Chinese gooseberry fruit shell extract as a green and cheap corrosion inhibitor for mild steel in acidic solution. J Mol Liq. 2019; 282:366-384. https://doi.org/10.1016/j.molliq.2019.03.011
34. Hsissou R, et al. Experimental, DFT and molecular dynamics simulation on the inhibition performance of the DGDCBA epoxy polymer against the corrosion of the E24 carbon steel in 1.0 M HCl solution. J Mol Struct. 2019; 1182:340-351. https://doi.org/10.1016/j.molstruc.2018.12.030
35. Haruna K, Obot IB, Ankah NK, Sorour AA, Saleh TA. Gelatin: a green corrosion inhibitor for carbon steel in oil well acidizing environment. J Mol Liq. 2018; 264: 515-525. https://doi.org/10.1016/j.molliq. 2018.05.058
36. Lahmady S, Anor O, Forsal I, et al. Investigation of ziziphus lotus leaves extract corrosion inhibitory impact on carbon steel in a molar hydrochloric acid solution. Port Electrochim Acta. 2023; 41:135-149. https://doi.org/10.4152/pea.2023410203.
37. Talfana A, Forsal I, Lahmady S. Inhibition of Copper Corrosion by Solanum elaeagnifolium Extract in 0.5 M $H_2SO_4$ Solution. Anal Bioanal Electrochem. 2024; 16(7):683-699. https://doi.org/10.22034/abec.2024. 714696.
38. Aslam R, Mobin M, Zehra S, Aslam J. A comprehensive review of corrosion inhibitors employed to mitigate stainless steel corrosion in different environments. J Mol Liq. 2022; 364:119992. https://doi.org/10.1016/j.molliq.2022.119992.
39. Thakur A, Kumar A. Sustainable inhibitors for corrosion mitigation in aggressive corrosive media: a comprehensive study. J Bio-Tribo-Corros. 2021; 7:1-48. https://doi.org/10.1007/s40735-021-00501-y.
40. Ali IH, et al. Adsorption and corrosion inhibition behaviour of oil extracted from Moringa peregrina leaves for carbon steel in acidic media: Experimental and computational studies. Int J Electrochem Sci. 2021; 16(8):210842. https://doi.org/10.20964/2021. 08.49.
41. Solmaz R, Salcı A, Dursun YA, Kardaş G. A comprehensive study on the adsorption, corrosion inhibition efficiency and stability of acriflavine on mild steel in 1 M HCl solution. Colloids Surf A Physicochem Eng Asp. 2023; 674:131908. https://doi.org/10.1016/j.colsurfa.2023.131908.
42. Bensouda Z, et al. Effect of Mentha piperita essential oil on mild steel corrosion in hydrochloric acid. Int J Electrochem Sci. 2018; 13(8):8198–8221. https://doi.org/ 10.20964/2018.08.79.
43. Gadow HS, Fakeeh M. Green inhibitor of carbon steel corrosion in 1 M hydrochloric acid: Eruca sativa seed extract (experimental and theoretical studies). RSC Adv. 2022; 12:8953-8986. https://doi.org/10.1039/D2RA01296K.
44. Anor O, et al. An experimental investigation of a date seeds hydro-acetonic mixture extract inhibitor for corrosion inhibition of carbon steel in an acidic medium at high temperatures. Biointerface Res Appl Chem. 2022;13(3):271. https://doi.org/10.33263/BRIAC133.271
45. Wei H, Heidarshenas B, Zhou L, Hussain G, Li Q, Ostrikov KK. Green inhibitors for steel corrosion in acidic environment: state of art. Mater Today Sustain. 2020; 10:100044. https://doi.org/10.1016/j.mtsust. 2020.100044
46. Shwetha KM, Praveen BM, Devendra BK. A review on corrosion inhibitors: types, mechanisms, electrochemical analysis, corrosion rate and efficiency of corrosion inhibitors on mild steel in an acidic environment. Results Surf Interfaces. 2024; 2024: 100258. https://doi.org/10.1016/j.rsurfi.2024. 100258.
47. Chapagain A, et al. Alkaloid of Rhynchostylis retusa as green inhibitor for mild steel corrosion in 1 M $H_2SO_4$ solution. Electrochem. 2022; 3(2):211–224. https://doi.org/10.3390/electrochem3020013.
48. Ituen E, Akaranta O, James A. Evaluation of performance of corrosion inhibitors using adsorption isotherm models: An overview. Chem Sci Int J. 2017; 18:1-34. https://doi.org/10.9734/CSJI/2017/28976
49. Al-Saeedi SI, Areej A, Qamar MT, Alhujaily A, Iqbal S, Alotaibi MT, Aslam M, Qayyum MA, Bahadur A, Awwad NS, Jazaa Y, Elkaeed EB. Isotherm and kinetic studies for the adsorption of methylene blue onto a novel $Mn_3O_4$–$Bi_2O_3$ composite and their antifungal performance. Front Environ Sci. 2023;11: 1156475. https://doi.org/10.3389/fenvs.2023.1156475.
50. Yousef TA, Hussein RK, Alhamzani AG, Al-Enazi AT, Al-Osimi MB, Abou-Krisha MM. Environment-friendly corrosion inhibitors for aluminum in hydrochloric acid: Quantum and experimental research. Metals. 2022; 12:1538. https://doi.org/10.3390/met12091538.
51. Akinbulumo OA, Odejobi OJ, Odekanle EL. Thermodynamics and adsorption study of the corrosion inhibition of mild steel by Euphorbia heterophylla L. extract in 1.5 M HCl. Results Mater. 2020;5:100074. https://doi.org/10.1016/j.rinma. 2020. 100074.



How to cite this article:
Talfana A, Kerouad S, Forsal I, Kotmani W, Kabiri L, ElHarami A, Ghazoui M. Natural Corrosion Inhibitor from Cistanche Tubulosa Extract for Carbon Steel in HCl: Gravimetric and Electrochemical Characterization. Prog Color Colorants Coat. 2026;19(1):67-82. https://doi.org/10.30509/pccc.2025.167509.1383.